PHYSICAL REVIEW C VOLUME 23, NUMBER 2 FEBRUARY 1981

Coulomb and nuclear inelastic excitations and the optical potential for heavy ions

M. A. Franey and P. J. Ellis
School of Physics and Astronomy, University of Minnesota, Minneapolis, Minnesota 55455
(Received 11 August 1980)

We present a simple, exact numerical method of obtaining the complex, l-dependent potentials $\Delta U_l(r)$ induced in the elastic channel by coupling to inelastic channels. For $^{16}O + ^{152}Sm$ at 72 MeV, we consider pure Coulomb coupling and find that a simple power law absorption or the imaginary l-dependent polarization potentials of Baltz *et al.* gives good agreement with coupled channel cross sections out to 100°. For larger angles a more accurate representation of the polarization potentials for the low partial waves is required, both real and imaginary parts being significant. We also examine the $^{13}C + ^{40}Ca$ system at 68 MeV including a number of excited levels in both projectile and target. Here, nuclear coupling is dominant. The strength of the imaginary part of ΔU_l is found to vary quadratically with deformation length and inversely with excitation energy for excitations above about 5 MeV. The states above 8 MeV lead to a real potential of strength comparable to the imaginary in the surface region. The effect on the cross sections is discussed.

[NUCLEAR REACTIONS $^{152}Sm(^{16}O,^{16}O')$, $E=72$ MeV; $^{40}Ca(^{13}C,^{13}C')$, $E=68$ MeV; coupled channel analysis; deduced effective elastic optical potential.]

I. INTRODUCTION

Heavy ion elastic scattering data[1-4] obtained at energies in the neighborhood of, or below, the Coulomb barrier have revealed a significant depletion of the Rutherford cross section forward of the grazing angle. Such an effect is not obtained with standard optical potentials. It can, however, be explained by coupled channels calculations which allow for the Coulomb excitation of low lying levels.

It is useful to incorporate these Coulomb excitation effects in an effective optical potential designed for pure elastic scattering calculations, i.e., to derive the polarization potential associated with Coulomb excitation. An l-independent form of this polarization potential has been obtained by Love, Terasawa, and Satchler[5] (LTS) in a plane-wave approximation. The potential is found to be primarily absorptive and to depend on the radial separation as $1/R^5$ (approximately); the long range nature of this potential, due to its origin in Coulomb excitation, is the new feature needed to describe the elastic scattering data. Subsequently Baltz *et al.*[6] (BGKP) have improved on this treatment by using Coulomb wave functions to devise an l-dependent potential (see also Donangelo *et al.*[7] for a semiclassical approach). Baltz *et al.* obtain in addition the cross sections for sub-Coulomb elastic and inelastic scattering in closed form. We also remark that Fröbrich *et al.*[8] have recently discussed the extraction of a polarization potential from the elastic component of the Coulomb excitation S matrix.

The present work is complementary to that of Refs. 5 and 6, since we adopt a purely numerical, although exact, approach. Specifically, we carry out coupled channels calculations involving elastic and inelastic scattering channels. The results are used to define effective optical potentials which produce the same elastic scattering wave functions and cross sections as the full coupled channels calculations. The effective potentials thus obtained are local, but l dependent. This procedure is discussed further in Sec. II, where we take as a first example the case of ^{16}O scattering from ^{152}Sm at 72 MeV. The Coulomb excitation mechanism is dominant here, so that it is appropriate to compare our exact numerical approach with the work of LTS and BGKP. We also suggest a simple procedure for averaging over the l dependence of our potential so as to produce an l-independent result. This procedure is found to work rather well in practice and bridges the gap between Ref. 5 and Ref. 6.

In Sec. III we turn to an example where the inelastic excitation is dominantly nuclear, rather than Coulomb. Rather little is known about such cases for heavy ion scattering, although a brief discussion of the $^{16}O + ^{40}Ca$ system was given by BGKP. Here we elect to study the case of ^{13}C scattering from ^{40}Ca at 68 MeV for a number of reasons. Firstly, elastic and inelastic cross sections are available for the low lying states.[9] Secondly, proton inelastic scattering on ^{40}Ca and ^{12}C has been studied[10,11] so that the inelastic excitation strengths to low lying levels are known. Thirdly, several groups[12-14] have studied the contributions of inelastic and transfer channels to the optical potential for protons scattering from ^{40}Ca. Lastly, the angular distribution for the $^{40}Ca(^{13}C, ^{14}N)^{39}K$ reaction at 68 MeV is known

to be anomalous[15] and it is conceivable that the present work could have some relevance to this problem. We shall make a fairly thorough study of the polarization potential induced by exciting a single level in ^{40}Ca and suggest a simple prescription to obtain an l-independent potential. We shall then discuss the polarization potentials obtained when a number of levels in ^{40}Ca and ^{13}C are included in the coupled channels calculations. We give a summary of our results in Sec. IV, along with some concluding remarks.

II. DOMINANT COULOMB EXCITATION EFFECTS

A. Calculational procedure

Consider the scattering for a two-channel system which can be described schematically by the following set of coupled equations:

$$(E_1 - H)\chi_1 = V_{12}\chi_2 , \tag{2.1}$$

$$(E_2 - H)\chi_2 = V_{21}\chi_1 + V_{22}\chi_2 . \tag{2.2}$$

The wave functions of the target-projectile relative motion, χ_1 and χ_2, describe the scattering when the target is in the zero-spin ground state (χ_1) and the excited level (χ_2). The coupling potentials V_{12} ($\equiv V_{21}$) and V_{22} are functions of the relative coordinate r and depend upon structure parameters such as the potential deformations β. The quantity V_{22} involves the matrix element of tensors of rank greater than zero acting on the target and relative motion wave functions; it is usually referred to as a reorientation term. It is zero if, for example, the excitation of a one-phonon vibrational state is considered as in Sec. III. The diagonal part of the Hamiltonian H includes the kinetic energy operator and the sum of the bare optical and Coulomb potentials, denoted by $U(r)$. In the usual way one obtains the set of coupled radial equations for each total J^π (determined uniquely by l_1 for the assumed spinless target and projectile):

$$\left\{\frac{d^2}{dr^2} - \frac{l_1(l_1+1)}{r^2} - \frac{2\mu}{\hbar^2}[U(r) - E_1]\right\}\phi_{l_1}(r) = \sum_{l_2} V^{L}_{12}(r)\phi_{l_2}(r) , \tag{2.3}$$

$$\left\{\frac{d^2}{dr^2} - \frac{l_2(l_2+1)}{r^2} - \frac{2\mu}{\hbar^2}[U(r) - E_2]\right\}\phi_{l_2}(r) = V_{21}\phi_{l_1}(r) + \sum_{L' l_2'} V^{L'}_{22'}(r)\phi_{l_2'}(r) . \tag{2.4}$$

The set is comprised of the elastic wave equation (2.3) and a number of equations like (2.4), one for each possible value of l_2.

The problem is posed as follows: Assuming the optical and coupling potentials are known, find the polarization potential $\Delta U_{l_1}(r)$, which solves

$$\left\{\frac{d^2}{dr^2} - \frac{l_1(l_1+1)}{r^2} - \frac{2\mu}{\hbar^2}[U(r) + \Delta U_{l_1}(r) - E_1]\right\}\phi_{l_1}(r) = 0 . \tag{2.5}$$

This defines the complex, local, l-dependent, trivially equivalent effective potential which reproduces the exact elastic wave function $\phi_{l_1}(r)$ (obtained from solving the coupled equations) in the case where the explicit coupling to the excited state is neglected.

We obtain $\Delta U_{l_1}(r)$ by solving (2.5) "backwards," that is, by inserting the elastic part of the coupled-channel wave function and numerically solving, for each value of r, the corresponding pair of algebraic equations for the real and imaginary parts, $\Delta U^{R}_{l_1}(r)$ and $\Delta U^{I}_{l_1}(r)$. This procedure is exact, direct, simple, and avoids the iterative necessities of Ref. 6. Furthermore, our method involves no additional complication when several excited states, or couplings between excited states, are included. The coupled equations were solved using the program CHORK.[16]

Having obtained the exact $\phi_{l_1}(r)$ we can return to Eq. (2.4) for the excited state wave function $\phi_{l_2}(r)$. In the absence of reorientation terms ($V_{22'} \equiv 0$), the right hand side is known so that we have an inhomogeneous equation to solve. Matching $\phi_{l_2}(r)$ to an outgoing wave yields the transition amplitude and hence the cross section in the usual way. This procedure is exactly equivalent[6] to carrying out a distorted-wave Born approximation (DWBA) calculation where the distorted waves in the ground state channel are generated with the potential $[U(r) + \Delta U_{l_1}(r)]$ and those in the excited state channel are obtained with the potential $U(r)$. Clearly this can be generalized to the case where we have several excited states provided that each state is coupled *only* to the ground state. Thus in Sec. III we can compare inelastic, as well as elastic, cross sections generated with approximate polarization potentials ΔU to the exact results.

B. The pure Coulomb case

As an example of strong Coulomb coupling we consider the scattering of ^{16}O by ^{152}Sm at E_{1ab} = 72 MeV. The elastic angular distribution obtained by Weber *et al.*[1] shows a smooth falloff below the Rutherford cross section (down to $\sigma/\sigma_R \sim 0.6$) at angles forward of the grazing peak near $\theta_{c.m.} \sim 85°$. The data have been fitted in coupled channel calculations carried out by Kim.[17] (Similar data have been analyzed for the

$^{18}O + ^{184}W$ system.[5,6])

For present purposes we wish to isolate the effects of strong Coulomb coupling. We therefore carry out coupled channel calculations with no nuclear potentials present. The "pure Coulomb" cross sections thus obtained are designated c data. Three examples of such data are shown in Fig. 1. In all cases the 0^+ ground state and 0.122 MeV 2^+ excited state of ^{152}Sm were coupled with a form factor of the form

$$V^L(r) = \frac{4\pi[B(EL\uparrow)]^{1/2}Z_{\text{Proj}}}{(2L+1)^{3/2}R_c^L} e \times \begin{cases} \dfrac{r^L}{R_c^{L+1}}, & r < R_c \\ \dfrac{R_c^L}{r^{L+1}}, & r \geq R_c \end{cases} \tag{2.6}$$

with $L=2$, $B(E2\uparrow)=3.45\ e^2b^2$, $R_c=9.82$ fm, and $Z_{\text{Proj}}=8$. The form factor needed for the reorientation terms was related to (2.6) by using the rotational model expression for $B(E2)^{1/2}$ values in a band. Integrations were carried out to 48 fm in steps of 0.08 fm for 201 partial waves. Comparison of the solid (without reorientation) and dashed (with reorientation) curves in Fig. 1 reveals the effect of reorientation on the elastic scattering when the channels are fully coupled. At angles $\theta_{c.m.} \lesssim 80°$ including reorientation produces a slower falloff below σ_R but changes the c data by less than 10%. However, at angles larger than this, the effect of reorientation is strong, resulting in cross sections an order of magnitude larger and an almost flat distribution for $\theta_{c.m.} \gtrsim 130°$.

It is also useful to compare with results obtained by treating the coupling in the two-step DWBA approximation (reorientation terms are not included in this order). The calculation was carried out by including three states, the ground state 0^+, the excited 2^+, and a second 0^+ state at zero excitation energy. The 2^+ was coupled "one way" from the ground state and the second 0^+ state was coupled one way from the 2^+. That is, the coupling potential V_{12} in Eq. (2.1) was set to zero but V_{21} in Eq. (2.2) was retained, and similarly for V_{23} and V_{32}. The partial wave scattering amplitudes for the two 0^+ states were then combined with the Rutherford scattering amplitude to calculate the elastic cross sections. This procedure thus allows only one scattering up to the 2^+ and then one scattering back to the ground state and is equivalent to a two-step DWBA calculation. The results, indicated by the dot-dash curve in Fig. 1, can be compared with the exact values, with and without reorientation. In the forward

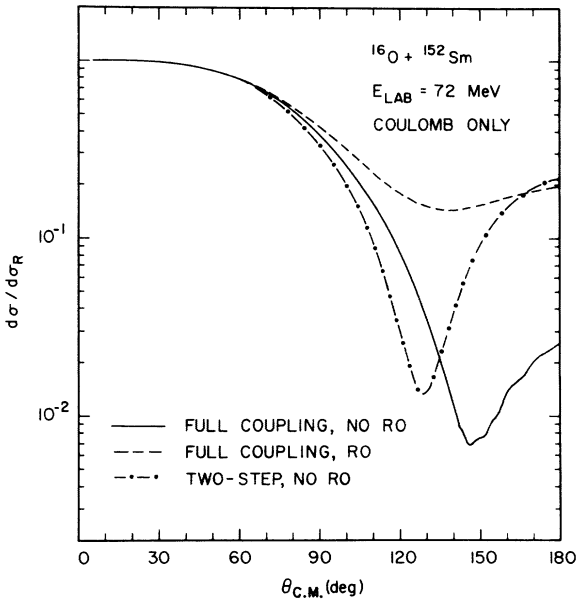

FIG. 1. "Pure Coulomb" c data for the $^{16}O + ^{152}Sm$ system at $E_{lab}=72$ MeV. The ground state is coupled to the 2^+ (0.122 MeV) excited state excluding reorientation (solid curve), including reorientation (dashed curve), and in a two-step DWBA (dot-dash curve).

angle region ($\theta_{c.m.} \lesssim 80°$) the differences are less than 10%. At larger angles the two-step DWBA fails to give a good approximation to either of the coupled channels results.

In order to compare our results more appropriately with those of LTS and BGKP, who neglect reorientation, we exclude the reorientation coupling henceforth. Figure 2 shows the exact imaginary polarization potentials $\Delta U_l^I(r)$ (for selected l's) corresponding to the solid curve in Fig. 1. Also shown are the BGKP potentials calculated with $B(E2\uparrow)=3.45\ e^2b^2$ and $g_2(\xi)=1.0$ (see Ref. 5 for notation). It is seen that $\Delta U_l^I(r)$ is absorptive in the interior rising smoothly to a maximum near R_c (where the excitation form factor peaks) and then generally decreasing with larger r. For the higher partial waves ($l \gtrsim 30$), this falloff in the exterior is very closely approximated by the BGKP potentials, except for spikes where the potential changes sign. These spikes occur at minima in the magnitude of the coupled-channel elastic wave function. For the lower partial waves, ΔU_l^I is strongly oscillatory and this is not reproduced by the BGKP potentials. Of course this is not surprising since the approximations made by BGKP were tailored to large l values.

The exact real polarization potentials $\Delta U_l^R(r)$ for $l=0$, 20, 40, and 60 are shown in Fig. 3. They are attractive in the interior rising to a peak near R_c and oscillating about zero in the

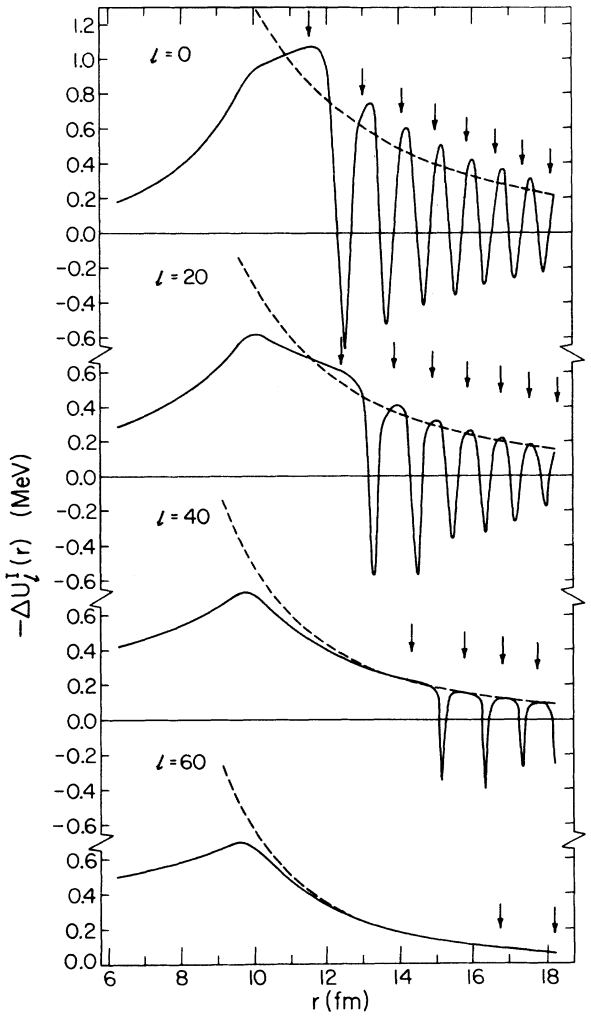

FIG. 2. Imaginary polarization potentials, $\Delta U_l^I(r)$, for the $^{16}O+^{152}Sm$ pure Coulomb case (without reorientation). The arrows mark values of r where $|\phi_l(r)|$ has maxima.

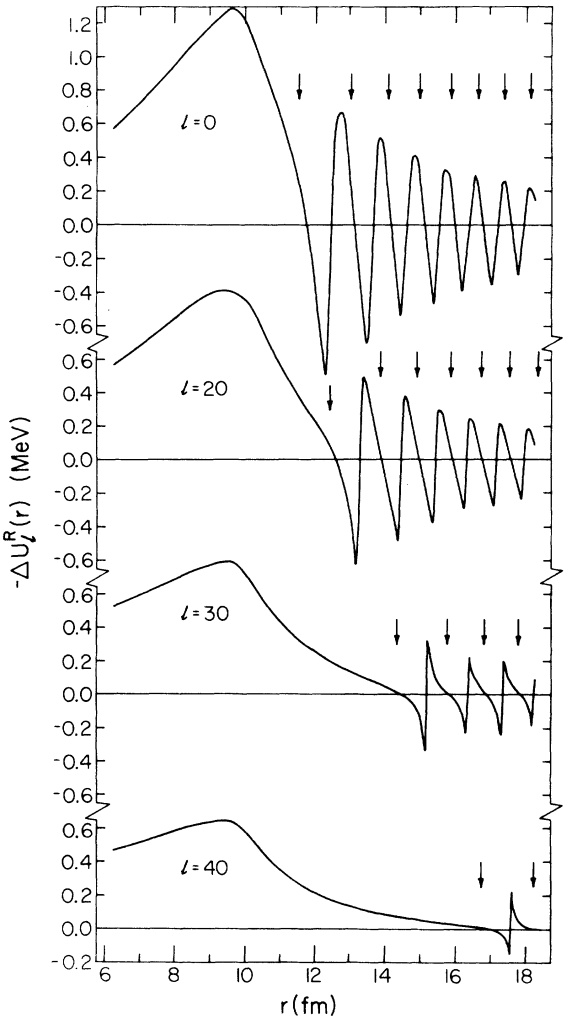

FIG. 3. As for Fig. 2, but the real polarization potentials, $\Delta U_l^R(r)$.

exterior. The general structure of the expression[6] for ΔU^R suggests that it would be roughly given by the ratio of an irregular to a regular Coulomb function. This would give rise to a cotangent behavior with the sign of ΔU^R changing at the minima in the magnitude of the elastic wave function. This is in qualitative agreement with the results in Fig. 3. One expects that these oscillating functions would contribute only "insignificant hair"[5,6] to the Coulomb plus centrifugal potential terms. This is evidently the case at large separations where the amplitude of $\Delta U_l^R(r)$ is $\lesssim 0.5$ MeV and $(E_{c.m.} - V_{Coul} - V_{Cent})$ is tens of MeV. However, near the classical turning point where the radial wave function is rising toward its first peak, $(E_{c.m.} - V_{Coul} - V_{Cent}) \sim 0$, and a $\Delta U_l^R(r)$ of a fraction of an MeV can have a significant effect. Indeed it happens that for the lower partial waves ($l \lesssim 30$) the *phase* of the S-matrix element S_l is strongly changed by excluding $\Delta U_l^R(r)$. This effect is displayed in Table I. It can be seen that the *magnitude* of S_L is also to some extent dependent on $\Delta U_l^R(r)$.

It is interesting to ask how the cross sections depend on the low partial waves. In Fig. 4 the solid curve was calculated using the complex, exact $\Delta U_l(r)$ for $l = 0$–30 and the BGKP purely imaginary, l-dependent potentials for $l = 31$–200. The fit to the c data (squares) is excellent. Comparison of the solid curve with the dot-dash curve which was calculated with the exact $\Delta U_l^R(r)$ for $l = 0$–30 and BGKP imaginary l-dependent potentials for $l = 0$–200 shows that inaccuracies in the BGKP approximations for the low partial waves are significant at the larger angles. However, for $l \gtrsim 30$ [where $\Delta U_l^R(r)$ is unimportant],

TABLE I. Magnitude and phase of the S-matrix element S_l for scattering of ^{16}O by ^{152}Sm with only Coulomb potentials present. The upper line for each l contains the exact S_l produced by $\Delta U_l^R + \Delta U_l^I$. The lower line contains the S_l obtained with ΔU_l^I only.

l	$\lvert S_l \rvert$	$\arg(S_l)$ (rad)
0	0.179	2.12
	0.142	0.02
10	0.120	1.37
	0.216	−0.05
20	0.273	0.18
	0.380	−0.10
30	0.503	−0.01
	0.556	−0.11
40	0.677	−0.06
	0.699	−0.10
60	0.862	−0.07
	0.866	−0.08
90	0.954	−0.05
	0.955	−0.05
150	0.991	−0.09
	0.991	−0.09

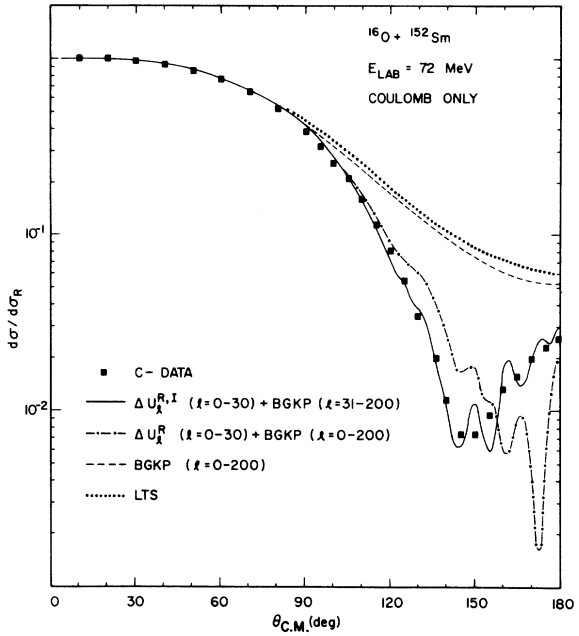

FIG. 4. Calculated cross sections for the $^{16}O + ^{152}Sm$ pure Coulomb case. The squares are the c data from a coupled-channel calculation (without reorientation). The curves show the single-channel predictions in various approximations.

the BGKP potentials accurately approximate the exact $\Delta U_l^I(r)$, and indeed for $l > 60$, the BGKP S-matrix elements are within 1% of the coupled-channel S_l. The dashed curve of Fig. 4 was calculated by using only the ΔU_l^I of BGKP. This produces cross sections considerably larger than the c data at angles beyond about 120°. The corresponding results obtained with the LTS potential (dotted curve) are very similar.

The dashed and dotted curves of Fig. 4 actually give quite a good approximation to the exact results including reorientation out to 130° (see dashed curve of Fig. 1). However, if reorientation effects are included in the BGKP potential following Hussein,[23] the dashed curve of Fig. 4 is pushed up at angles beyond 90°. This is not sufficient to give agreement with the exact results at extreme backward angles and leads to poorer agreement in the 90–120° region. Furthermore, it is clear that for angles beyond about 100° the lower partial wave potentials must be more accurately represented and, in particular, the *real* effective potential is not negligible. Thus several opposing effects come into play at large angles so that the close agreement between the approximate BGKP treatment and the exact results (with reorientation) must be regarded as fortuitous. Of course, in actual considerations of large angle data at this energy the effect of nuclear potentials in the low partial waves must be considered, and this is discussed in Sec. IIC.

While the LTS and BGKP potentials are adequate for regions forward of 80°, as we have remarked, it nevertheless is useful to consider a simple phenomenological approach here. Specifically we fit the c data with a simple power law polarization potential of the form

$$\Delta U^{I,n}(r) = \begin{cases} -\dfrac{U_{on} r^{n-2}}{R_c^{(2n-2)}}, & r < R_c \\ -\dfrac{U_{on}}{r^n}, & r \geq R_c . \end{cases} \tag{2.7}$$

The shape of the potential inside R_c (= 9.82 fm) has been chosen to simulate the square of the Coulomb excitation coupling form factor [Eq. (2.6)], although the cross sections are insensitive to the potential inside 10 fm.

A free search on n and U_{on} gives $n = 6.38$ and $U_{on} = 2.65 \times 10^{6.38} = 6.36 \times 10^6$ MeV. This potential fits the c data from $\theta_{c.m.} = 0$–80° with a χ^2 per point of 0.3, assigning "errors" of 1% to the c data. By gridding on n and adjusting U_{on} for a best fit, it is found that the important absorptive region is centered around 16 fm where the c data require $\Delta U^{I,n}(16) \sim -0.12$ MeV.

We calculated the elastic scattering using the exact $\Delta U_l(r)$ for $l = 0$–30 and $\Delta U^{I,6.38}$ for $l = 31$–200. It is essentially identical to the solid curve of Fig. 4 which employed the BGKP l-dependent potentials for $l = 31$–200. Although the

cross sections for these two calculations differ by less than a couple of percent, it should be pointed out that the S_l from the power law $\Delta U^{I,6.38}$ differ in magnitude from those of the BGKP potentials by + 2% ($l=40$), −15% ($l=100$), and −40% ($l=150$).

It has been noted[6] that all of the l-dependent potentials of BGKP [and also the exact $\Delta U_l^I(r)$] fall off considerably more slowly than either the $r^{-5.8}$ (near 16 fm, including the so-called Coulomb braking) of the LTS potential or the $r^{-6.4}$ of the phenomenological potential. However, the l-dependent potentials may be reconciled with the l-independent ones by noting that an approximate effective l-independent absorption $\Delta U^I(r)$ can be generated by requiring ΔU^I to be approximately correct (at each r) for the partial wave most affected by the potential near that separation. For example, consider the $l=0$ radial wave function which first peaks at 11.5 fm and the $l=90$ wave function which has its first maximum at 20.7 fm. Because of the large centrifugal repulsion, $\phi_{90}(r)$ is insensitive to the potential near 11.5 fm, so $\Delta U^I(r)$ can be chosen to be close to $\Delta U_0^I(r)$ in that region. Conversely, $\phi_0(r)$ is little affected by the potential near 20.7 fm, where $\phi_{90}(r)$ is most sensitive, and thus $\Delta U(r)$ near this separation should be close to $\Delta U_{90}^I(r)$.

A prescription based on the idea of choosing the l-independent potential to be appropriate to larger partial waves as r increases can be given in the following way.

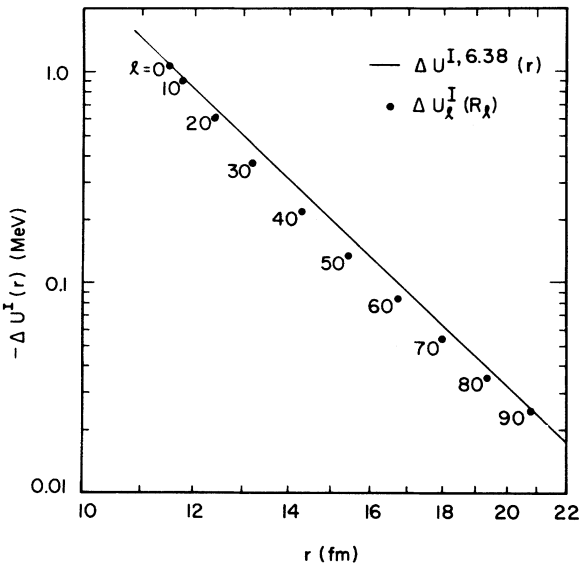

FIG. 5. Plot of the power law polarization potential $-\Delta U^{I,6.38}(r)$. The dots correspond to $-\Delta U_l^I(R_l)$ for various l, where R_l is the value of r at which $|\phi_l(r)|$ has its first maximum.

(1) Determine the distance R_l at which the first maximum in the lth partial wave occurs.

(2) Plot $\Delta U_l^I(R_l)$ vs R_l and interpolate to obtain $\Delta U^I(r)$.

It is very satisfying that $\Delta U^I(r)$ generated in this physically reasonable way (see Fig. 5) is very close to $\Delta U^{I,6.38}(r)$, the best fit power absorption. It is found that $\Delta U^I(r)$ has an average logarithmic slope (i.e., power of r) of −6.3, but is about 15% too low in magnitude.

C. Combined Coulomb and nuclear coupling

Here we consider the effect of nuclear coupling in the presence of a strong Coulomb interaction for the $^{16}O+^{152}Sm$ system at $E_{lab}=72$ MeV. The c data (squares in Fig. 6) were generated as in Sec. IIB except that a nuclear potential was included and both Coulomb and nuclear ($\Delta L=2,4$) reorientation terms were retained. We used the optical parameters of Kim,[17] which are listed as Set A in Table II, together with $\beta_2=0.219$ and $\beta_4=0.0385$ and included only the 0^+ ground state and first excited 2^+ level. Diagonal and off-diagonal radial form factors were obtained from the full multipole expansion of the optical potential.

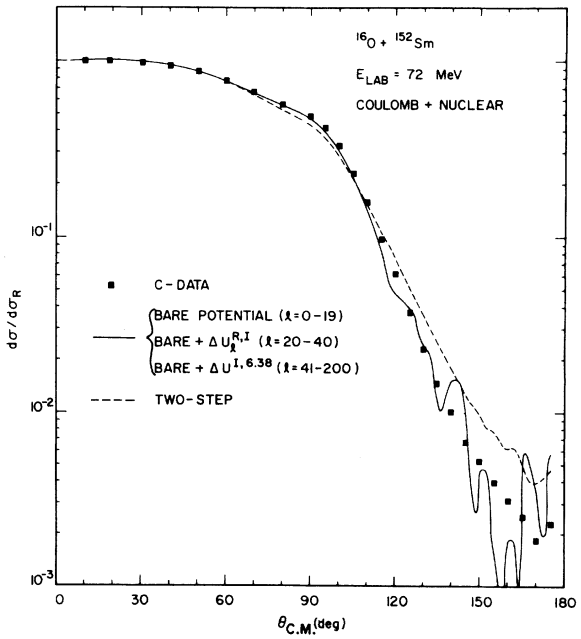

FIG. 6. Cross sections for the $^{16}O+^{152}Sm$ system at $E_{lab}=72$ MeV including nuclear and Coulomb potentials (with reorientation). The squares are coupled-channel c data. The solid curve gives the single-channel predictions using the bare potential plus ΔU_l for $l=20$–40 and $\Delta U^{I,6.38}$ for $l=41$–200. The dashed curve gives the two-step DWBA predictions using the full nuclear and Coulomb coupling.

TABLE II. Parameters of the optical potentials.

Parameter set	V (MeV)	r_R (fm)	a_R (fm)	W (MeV)	r_I (fm)	a_I (fm)	r_c (fm)
			$^{16}O + ^{152}Sm$				
A	13.0	1.37	0.50	4.5	1.40	0.58	1.25
			$^{13}C + ^{40}Ca$				
B	33.6	1.30	0.55	12.0	1.30	0.55	1.27
C	39.6	1.31	0.52	10.3	1.46	0.38	1.27

Three features of the elastic angular distribution can be correlated approximately with individual parts of the interaction. That is, the smooth decrease in cross section out to $\theta_{c.m.} \sim 80°$ is determined by the Coulomb coupling between the two states; the plateau near $\theta_{c.m.} = 85°$ is a result of the *nuclear* off-diagonal coupling; and the rather steep falloff at angles beyond $\theta_{c.m.} \sim 90°$ is due chiefly to the diagonal nuclear potential. These angular effects correspond to the following considerations in angular momentum space. The larger partial waves ($l = 41-200$) are little affected by the nuclear potentials or reorientation couplings and are therefore well described by the Coulomb polarization potentials of Sec. IIB; the grazing waves ($l = 20-40$) are significantly affected by the nuclear coupling; and the smaller partial waves ($l = 0-19$) are so damped by the diagonal absorption that their corresponding $\Delta U_l(r)$ have a relatively small effect on the cross sections. These features are demonstrated by the good fit (Fig. 6) to the c data obtained by adding to the bare potential: no polarization potential for $l = 0-19$, the exact polarization potential $\Delta U_l^{R,I}(r)$ for $l = 20-40$, and the imaginary Coulomb polarization potential $\Delta U^{I,6,38}(r)$ of Sec. IIB for $l = 41-200$. The corresponding DWBA inelastic scattering predictions are in similar excellent agreement with the inelastic c data. The dashed curve in Fig. 6, which was obtained in a second order DWBA calculation, is in much better agreement with the c data than in the pure Coulomb case. Thus, higher order effects, such as reorientation, are less significant when the nuclear potential is present.

The polarization potentials $\Delta U_l(r)$ obtained in these calculations are shown in Figs. 7(a) and 7(b). As might be expected from the discussion above, the polarization potentials are strongly damped in magnitude for the low partial waves, while for $l = 40$, and beyond, they are similar to the ΔU_l obtained in the pure Coulomb case. For the grazing waves ($l \approx 30$), the $\Delta U_l^R(\Delta U_l^I)$ found here are similar in shape to the $\Delta U_l^I(\Delta U_l^R)$ of the pure Coulomb case. For instance, $\Delta U_{30}^R(r)$ peaks at separations which correspond to maxima in $|\phi_{30}|$, whereas in the pure Coulomb case the imaginary part showed this behavior. This suggests that the real potential significantly affects the cross sections and this is found to be the case at angles in the region of the grazing bump and beyond 120°.

III. NUCLEAR POLARIZATION POTENTIAL

In this section we consider a case where nuclear effects dominate the inelastic excitation. For the reasons explained in the Introduction, we elect to study ^{13}C scattering from ^{40}Ca at 68 MeV. In our calculations we use the optical potential parameters of Bond *et al.*[9] which are listed as Set B in Table II. The coupling potential is generated by allowing the nuclear surface to vibrate and expanding to first order in the deformation in the usual way.[18] Thus we have no reorientation couplings and the form factor for inelastic excitation is given by the first derivative of the optical potential. The employed deformation lengths βR are discussed below. We also allow Coulomb excitation, but this produces a very small effect. Integrations were carried out to 25.2 fm in steps of 0.08 fm for 81 partial waves.

We note that the parameters of Bond *et al.*[9] were obtained by coupled channels fits to the data for the 0^+ ground state, the 3.73 MeV 3^-, and the 4.48 MeV 5^- levels of ^{40}Ca. Thus these parameters should produce physically reasonable results. This is our main concern here, since we are interested in qualitative trends rather than detailed comparison to data.

A. Effect of single states in ^{40}Ca

First we consider coupled channels calculations which involve the 0^+ ground state and 3.73 MeV 3^- level. The data[9] yield a deformation length $\beta_3 R = 1.05$ fm for the inelastic coupling. However, in order to accentuate the coupled channel effects for the purpose of illustration, we have increased this value by about a factor of 2. We take $\beta_3 R = 2.22$ fm. The deformation used for Coulomb ex-

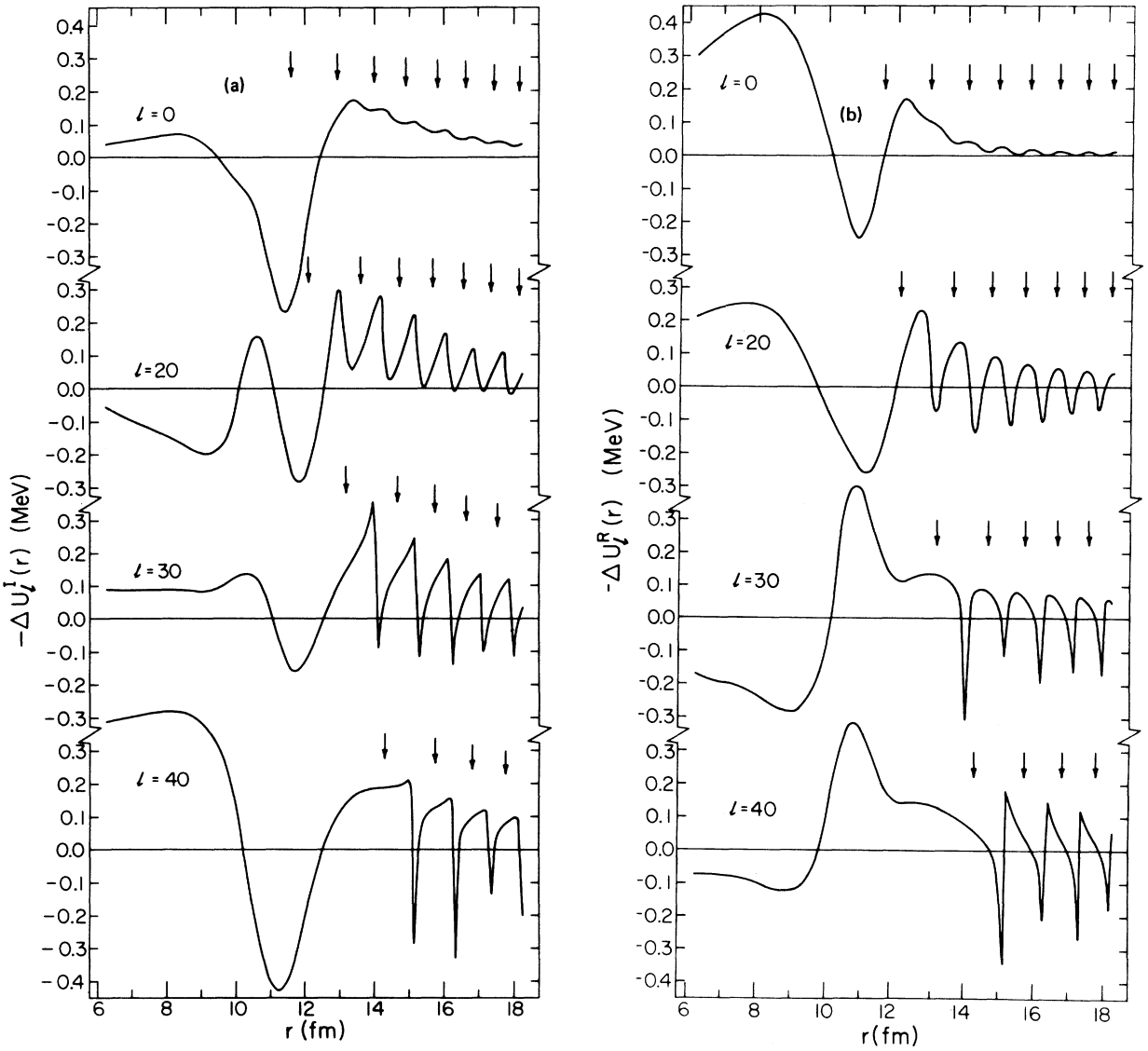

FIG. 7. The (a) imaginary polarization potentials, $\Delta U_l^I(r)$, and (b) real polarization potentials, $\Delta U_l^R(r)$, obtained for the case of $^{16}O+^{152}Sm$ including nuclear and Coulomb potentials. The arrows mark values of r where $|\phi_l(r)|$ has maxima.

citation was kept at the value obtained from the measured $B(E3)$.[19] The imaginary and real parts of the polarization potential $\Delta U_l(r)$ that we obtain are shown in Figs. 8(a) and 8(b), respectively, for a few selected partial waves. The dashed lines in these figures show the appropriate component of the bare optical potential $U(r)$, set B of Table II. The results are clearly l dependent with $|\Delta U_l|$ peaking for the surface partial waves. (The magnitude of the elastic scattering matrix element $|S_l|$ has the value 0.5 at a critical angular momentum of 34.5.) The imaginary part of ΔU_l is absorptive almost everywhere, whereas the real part changes from repulsive to attractive as l increases. This is quite similar to the case[6] of ^{16}O scattering from ^{40}Ca. For $l \sim 34$, we see that the imaginary component $\Delta U_l^I(r)$ obtained here exceeds the bare potential between 7 and 9 fm. This is the region which is significantly sampled by the ^{13}C scattering. On the other hand, the real part $\Delta U_l^R(r)$ changes sign in this region and is smaller in magnitude than the bare potential. It is therefore to be expected, and indeed is found, that the imaginary part of $\Delta U_l(r)$ provides the dominant effect.

It is not obvious that an l-independent potential $\Delta U(r)$ can be found which will give a reasonable approximation to the coupled channel elastic

and inelastic cross sections. We have examined various methods of averaging over our calculated l dependence and we conclude that what is needed is a weighting which emphasizes the surface partial waves. In our calculations we use a weighting factor $\exp\{-4(\ln 2)[(l-34)/6]^2\}$, i.e., a Gaussian peaked at $l=34$ with a full width at half maximum (FWHM) of 6 units of l. However, the results are not very sensitive to the precise form of the weighting provided that the surface partial waves dominate. The results obtained by this procedure are illustrated in Fig. 9. The heavy dotted "data points" show the coupled channel results. The dashed curves show for the ground state a pure elastic scattering calculation with the bare potential $U(r)$ (Set B, Table II) and, for the 3^- level, the cross section obtained in the DWBA. The dotted curves show the same calculations, but with $U(r)+\Delta U(r)$, i.e., including the approximate l-independent polarization potential. Note that this differs from the usual treatment in that we use $U+\Delta U$ for the elastic optical potential appropriate to the 0^+ ground state and U alone for the other potentials needed. As explained in Sec. IIA, this form of the DWBA will yield the exact coupled channel cross sec-

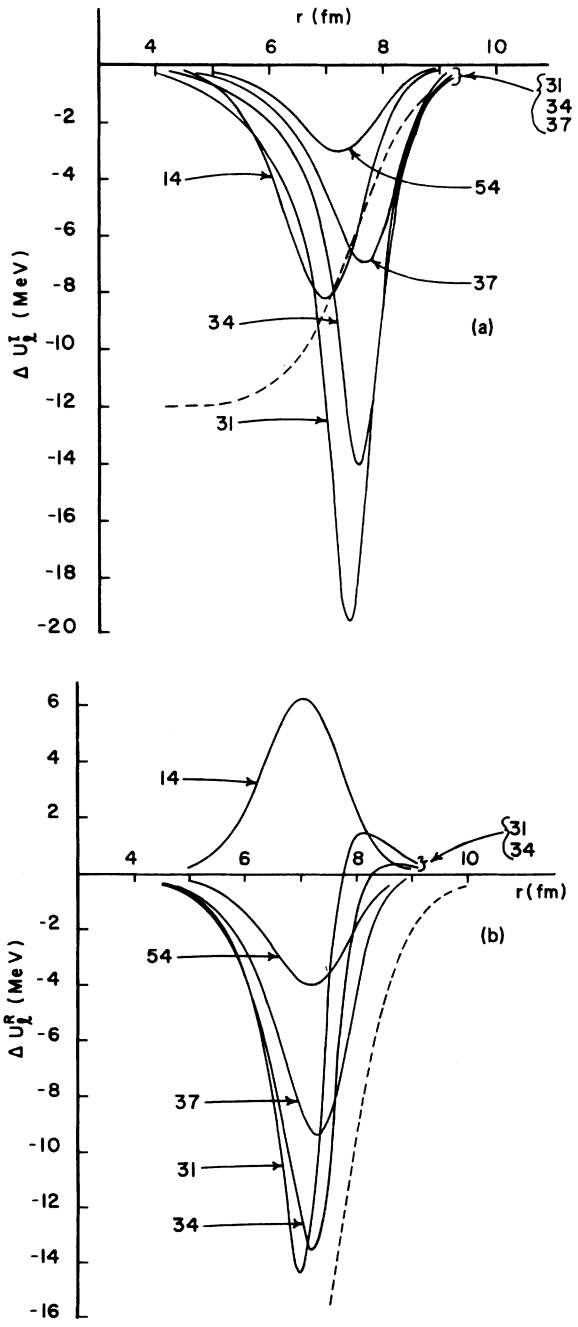

FIG. 8. The (a) imaginary part of the polarization potentials, $\Delta U_l^I(r)$, and (b) real part of the polarization potentials, $\Delta U_l^R(r)$, induced by the inelastic excitation of a single level for the $^{13}C+^{40}Ca$ system. Results are shown for a few selected partial waves; the bare potential is also shown (dashed curve).

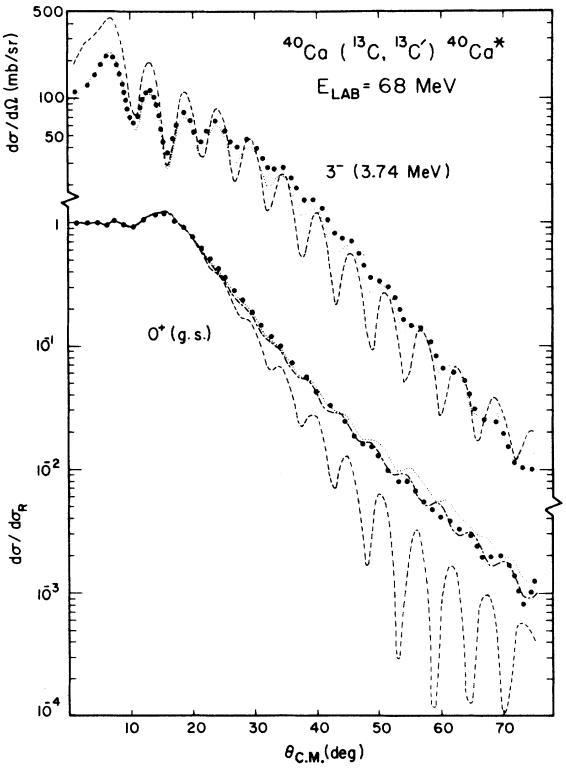

FIG. 9. Elastic and inelastic cross sections for the $^{13}C+^{40}Ca$ system. The results of calculations (see text) with the bare and bare plus polarization potentials are indicated by the dashed and dotted curves respectively. The heavy "data points" are the result of coupled channel calculations. The dot-dash curve gives the result of an optical model fit.

tion for the 3^- state if the exact polarization potential ΔU_l is used. Clearly the dotted curves give a reasonable approximation to the full coupled channel results, whereas the results obtained with the bare potential alone are vastly different.

We mention in passing that the effect of coupling, which we simulate by a predominantly imaginary ΔU, is an increase in the magnitude of the elastic cross section (for the angular range shown, something of the opposite trend appears for the large angles). This is surprising since it differs from the usual experience in light ion scattering. We have verified that the large Coulomb potential for heavy ions is necessary to achieve this effect. However, we have not found a complete explanation, although if we apply the model of Frahn and Gross[20] we find that the critical angle is larger for the $U+\Delta U$ case than for U alone. This has the effect of reducing the far side contribution (the oscillations are damped) and enhancing the near side contribution.

It is interesting to enquire whether the coupled channel elastic cross section can be fitted by a variation of the parameters of the phenomenological optical model. As expected, we found that changes in the real part of the potential are of minor importance. Regarding the imaginary part, comparable fits can be obtained by adding a surface peaked term (standard first derivative Woods-Saxon) to Set B of Table II or by simply modifying the volume term. The latter yields Set C of Table II and the fit is illustrated by the dot-dash curve in Fig. 9. It is surprisingly good, given the surface nature of the polarization potential. The important point seems to be an enhancement of the imaginary potential in the 8–9 fm region.

Thus far we have coupled the ground state to a level with $J^\pi = 3^-$. If instead we couple to single levels with $J^\pi = 2^+$, 4^+, or 5^-, the remaining parameters of the calculation being unchanged, we find that quite similar polarization potentials are obtained. Also the qualitative trends of the cross sections are similar to those of Fig. 9. For reasons of economy, we therefore consider coupled channels calculations involving the 0^+ ground state and a 2^+ level at a variable excitation energy E_x, excited with various deformations β_2. (The "physical" value for the nuclear deformation is taken from Ref. 9 and the physical value for the Coulomb deformation is taken from Ref. 19 and the two are scaled together.) We show in Fig. 10, for various β_2 and E_x, the magnitude of the imaginary polarization potential at 8.56 fm for the $l = 35$ partial wave. This should be sufficient to display the significant trend of the results. Firstly, for a given E_x, we see that the points fall quite accurately on straight lines, i.e., the polarization potential is proportional to β^2. This is a trivial result for the nonlocal form of the potential,[12] but not for the equivalent local potential. One might, in fact, have expected some change from linearity since β_2^2 ranges up to 0.40 corresponding to $\beta_2 R = 2.81$, whereas the physical (nuclear) value of $\beta_2 R$ is 0.41. It can also be seen from Fig. 10 that the polarization potential falls off as a function of E_x approximately as E_x^{-1}, for $E_x \gtrsim 5$ MeV. Below this value of E_x the magnitude of the polarization potential levels off.

Now, in practice, the strength of a single level may be spread over several levels, so we have explored the effect of fractionation on the polarization potential. Firstly, we have compared the polarization potential obtained from a coupled channel calculation involving the 0^+ ground state and three 2^+ levels with the sum of the ΔU obtained in three separate coupled channel calculations involving the 0^+ and each 2^+ in turn. The agreement is quite reasonable in the cases we have examined (to within 10% beyond 8 fm), although since the nonadditivity results from the reduction to an equivalent local potential it will clearly depend on the strength of the coupling. Making the additivity assumption, ΔU^I will be proportional to $\sum_i \beta_2(i)^2/E_x(i)$, whereas the energy weighted sum rule conserves $\sum_i \beta_2(i)^2 E_x(i)$. It therefore appears that ΔU^I would be rather sensitive to the precise distribution of strength. In fact, however, this sensitivity is not very great in a realistic case. We have in mind a single level at a reasonably high excitation energy, say ~15 MeV, whose strength is symmetrically distributed over a series of levels in the 10–20 MeV

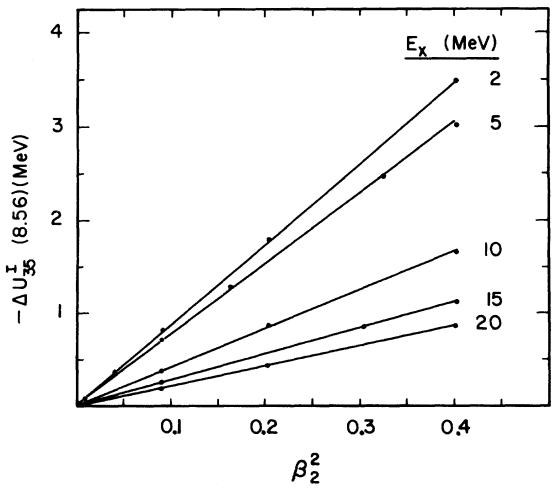

FIG. 10. For the case of $^{13}C+^{40}Ca$, the β_2 dependence of $\Delta U^I_{35}(8.56)$ is displayed for several values of the excitation energy E_x of a 2^+ level.

range, as, for example, in Ref. 12. Provided that the energy weighted sum rule is satisfied, the polarization potentials in the single level and multilevel cases differ by less than 10% in the examples we have studied. Thus the sensitivity to the distribution of strength is probably no more marked here than in the light ion case.[12] Note that this conclusion rests heavily on the assumption of a symmetrical strength distribution.

B. Effect of several states in ^{40}Ca and ^{13}C

Here we consider the effect of including in the coupled channel calculations a number of excited states in the ^{13}C + ^{40}Ca system. These states are listed in Table III. Below 10 MeV in ^{40}Ca they represent levels, or groups of levels, which are strongly excited in inelastic proton scattering.[10] In some cases[9] the deformation lengths $\beta_\lambda R$ could be taken from measurements of the inelastic scattering of ^{13}C. In other cases deformation lengths were taken from the proton data[10] and these were multiplied by factors 1.0, 0.78, and 0.65 for multipolarities λ of 2, 3, and 4, respectively, on the basis of the results given in Ref. 9. These factors correct for the fact that the conventional derivative form factors, which we use, are independent of λ, whereas the folding model[21] and the data[9] indicate that the magnitudes should depend on the multipolarity for heavy ion scattering. The remaining states in ^{40}Ca were placed, somewhat arbitrarily, in the neighborhood of 20 MeV with deformation lengths chosen to exhaust the energy weighted sum rule.[22] Using a radius parameter $R = 4.45$ fm, the deformations β_λ in Table III were thus obtained.

The calculations we have carried out thus far have been independent of the spin of ^{13}C. Were we to take into account the important states in ^{13}C with their actual spin values the calculation would become intractable. Instead we have chosen to represent the spectrum of ^{13}C by that of ^{12}C thus ignoring the presence of the extra particle. This should be sufficiently accurate for the collective excitations in which we are interested here. We therefore take the ground state to have zero spin and use the excited states and deformations listed in Table III. These are derived from the compilation of Ajzenberg-Selove, the hadron inelastic scattering work of Buenerd *et al.*,[11] and the energy weighted sum rule as in the case of ^{40}Ca. Here, however, the radius parameter $R = 2.98$ fm.

Coulomb excitation was included in the calculations, but it is a small effect; the values of the Coulomb deformations were derived from electromagnetic data, where known, and scaled according to the nuclear deformations otherwise. The optical parameters used are as listed under Set B in Table II, except where noted.

Using various combinations of the states in Table III we have derived l-independent polarization potentials ΔU. The averaging over l was carried out with the procedure discussed in Sec. III A; this appears to be reasonable for the surface partial waves in the 7–9 fm region, although here we cannot compare with exact results since it was only possible to perform these large coupled channel calculations for a few partial waves. Some selected polarization potentials are shown in Figs. 11(a) and 11(b).

The behavior of the imaginary component ΔU^I [Fig. 11(a)] is straightforward—it essentially just scales according to $\sum_i \beta_\lambda(i)^2 R_i^2 / E_x(i)$, where R_i is the radius parameter appropriate to ^{40}Ca or ^{13}C. If we compare the case where all the states of Table III are included to the case where just the ^{40}Ca 3^- level is involved, we get a scaling factor of about 6 and the actual curves give this ratio at ~8 fm. Clearly this is a large enhancement. The largest individual contribution is given by the 4.44 MeV 2^+ state of ^{12}C; the 3.74 MeV 3^- level of ^{40}Ca is also strong. However, the effect

TABLE III. States included in the coupled channel calculations of ^{13}C + ^{40}Ca. The states of ^{12}C are used to represent the inelastic excitation of ^{13}C.

^{40}Ca			^{12}C		
E_x (MeV)	Multipolarity λ	Deformation β_λ	E_x (MeV)	Multipolarity λ	Deformation β_λ
3.74	3	0.24	4.44	2	0.53
3.90	2	0.09	9.64	3	0.31
4.48	5	0.10	14.1	4	0.08
7.5	4	0.08	27.0	2	0.51
8.0	2	0.13	27.0	3	0.59
8.0	3	0.11	27.0	4	0.68
18.0	2	0.23			
20.0	3	0.23			
20.0	4	0.28			

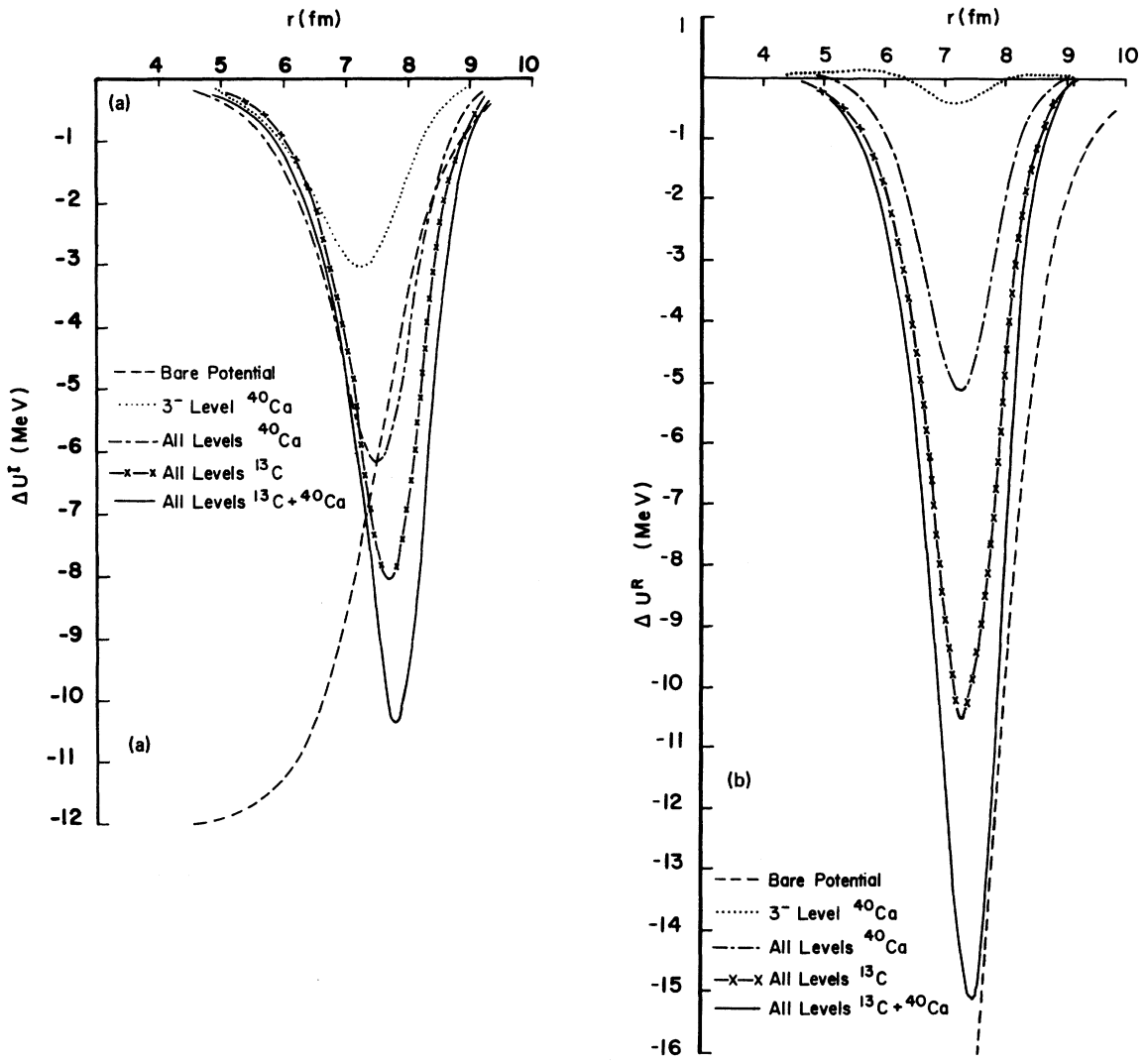

FIG. 11. The (a) imaginary part of the polarization potentials, $\Delta U^I(r)$, and (b) real part of the polarization potentials, $\Delta U^R(r)$, induced by the inelastic excitation of various levels in the $^{13}C+^{40}Ca$ system. The bare potential is also shown (dashed curve).

of all the other levels, including those at high excitation energy, is significant. It should be clear that excitations of both the projectile and the target are important, with the former being somewhat larger in this case.

The behavior of the real part ΔU^R [Fig. 11(b)] is less obvious. The states with $E_x < 8$ MeV produce a polarization potential which goes through zero in the 8–8.5 fm region. The higher levels, however, give a large amount of attraction in the surface region which shifts the zero out to larger distances. Thus the complete ΔU^R, with all states included, is dominantly attractive and becomes comparable to the imaginary part ΔU^I. It is not surprising that this ΔU^R produces a sizable effect on the calculated cross section, although still less than that given by ΔU^I.

The cross sections produced by the bare potential and the bare plus various polarization potentials in the DWBA are shown in Fig. 12. As the polarization potentials increase, i.e., as more levels in the $^{13}C+^{40}Ca$ system are included, the elastic cross section becomes less oscillatory and increases at the larger angles. We also see a corresponding diminution of the forward angle cross section for the 3.74 MeV 3^- state of ^{40}Ca; similar behavior is found for the inelastic excitation of the 3.90 MeV 2^+ and 4.48 MeV 5^- levels of ^{40}Ca (not illustrated). For reasons of clarity the results obtained from polarization potentials which include only the effect of the levels considered in ^{13}C are not shown. The cross sections

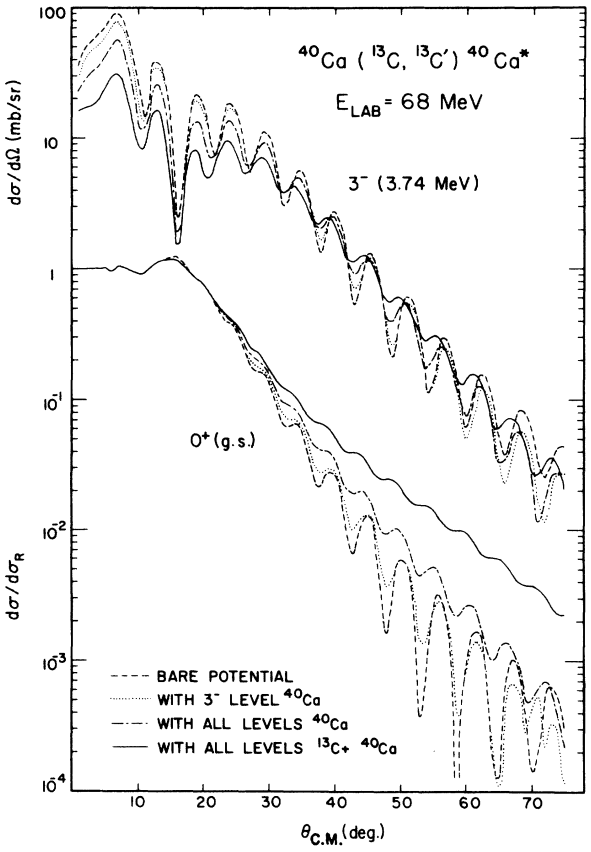

FIG. 12. Elastic and inelastic cross sections for the $^{13}C+^{40}Ca$ system. The results shown are obtained in optical model and DWBA calculations (see text) using the bare potential and the bare plus the various polarization potentials of Fig. 11.

are found to lie between those obtained by including all levels in ^{40}Ca (dot-dash curve of Fig. 12) and those obtained by including all levels in the $^{13}C+^{40}Ca$ system (full curve). This is to be expected from the relative sizes of the polarization potentials shown in Fig. 11.

Now the imaginary part of the phenomenological elastic optical potential is intended to take into account the flux lost in exciting the channels we have considered as well as the many other possible channels. The real part will also include the effect of the polarization potentials. Thus we should, in principle, use a modified optical potential U' in our calculations which would lead to the same elastic scattering and inelastic (DWBA) cross sections as obtained with the original bare potential U. We use the modified potential U' for the elastic scattering in the ground state and for the inelastic coupling. However, for elastic scattering in the excited states we use the original potential U since one can imagine that, just as for the ground state, each excited state has built on it a series of levels to which it is inelastically coupled. Such effects are included phenomenologically by using U rather than U'. We have not carried out a detailed fit to obtain U', but have simply considered modifications of the imaginary parameters W and r_I. Furthermore, the following remarks should be regarded as qualitative since we have only obtained a rough fit to the original cross sections. We find that it is necessary to reduce the imaginary strength W to about 2 MeV if r_I is unchanged. Similar results can be obtained with a larger value of W if the imaginary radius r_I is also reduced, e.g., $W=4$ MeV, $r_I=1.0$ fm. As regards the polarization potentials this significantly reduces ΔU^I, e.g., at 8.5 fm by about a factor of 2. However, ΔU^R is little changed. While these considerations are crude, they do suggest that inelastic excitation of a few strong states in the target and projectile can account for a surprisingly large part of the empirical imaginary optical potential.

IV. CONCLUSIONS

We have described a simple numerical procedure whereby the local, l-dependent polarization potential is obtained by inserting the elastic component of the coupled-channel wave function into the uncoupled Schrödinger equation. This method is exact and does not necessitate neglecting couplings (including reorientation terms) between excited levels. We then applied this procedure to two cases of heavy-ion scattering.

Firstly, we have examined the $^{16}O+^{152}Sm$ system at 72 MeV in the case where only Coulomb potentials were present. We find that coupled channel calculations including the 0^+ ground and 2^+ first excited state of ^{152}Sm require an imaginary $\Delta U^I(r) \propto r^{-6.38}$. A similar dependence is obtained by taking the values of the BGKP[6] $\Delta U_l^I(r)$ at the first maximum of a given partial wave to define an l-independent potential. While these polarization potentials reproduce the coupled channel elastic cross section up to 100°, the larger angles require a real component ΔU^R and a more accurate representation of ΔU^I for the lower partial waves. Thus n-step processes with $n>2$ are significant and this includes reorientation terms. These effects are ameliorated when nuclear potentials are included in addition to the dominant Coulomb potentials. The low partial waves are strongly damped; however, an accurate treatment of ΔU for the grazing partial waves is still clearly required.

We next turned to a case where nuclear effects dominate, namely $^{13}C+^{40}Ca$ at 68 MeV. In studies with a single excited level the ΔU are found to

be strongly l dependent, but the coupled channels results are quite well reproduced with an l-independent ΔU for which the surface partial waves are strongly weighted. We do not suggest that this is necessarily a universal prescription, but it is at least a compact way of presenting our results. We have studied the effect of including low levels which are known to be strong in inelastic excitation, together with high lying levels chosen to exhaust the energy weighted sum rule, in both ^{40}Ca and ^{13}C (which is treated as a ^{12}C nucleus). The largest single effects come from the 4.44 MeV 2^+ state of ^{12}C and the 3.73 MeV 3^- level of ^{40}Ca, but all of the states give significant contributions. As more states are included the imaginary component ΔU^I becomes increasingly absorptive and scales approximately according to $\sum_i [\beta_\lambda(i) R_i]^2 / E_x(i)$, where $\beta_\lambda R$ is the deformation length. For the real part, the levels below 8 MeV give a ΔU^R which changes sign in the surface, but the higher states give an attractive surface-peaked potential which is comparable to ΔU^I in the important 8–9 fm region. We have considered modifications of the bare potential so that ($U' + \Delta U'$) gives crudely similar cross sections to those obtained previously with U. This requires a surprisingly strong reduction in the imaginary strength (from 12 to 2 MeV) or less of a reduction in the strength together with a reduction in the imaginary radius.

Finally, we remark that we have carried out a few exploratory calculations for ^{13}C + ^{40}Ca including a real spin-orbit component U_{so} in the bare potential. Only the ground state and 3.73 MeV 3^- level of ^{40}Ca were included. We find that the real and imaginary parts of the deduced spin-orbit polarization potential ΔU_{so} are fairly similar. Further U_{so} and ΔU^R_{so} show some cancellation in the surface region so that the net spin-orbit term tends to shift from a real to an imaginary character. However, there appears to be no significant enhancement of the spin-orbit strength.

This research was supported in part by the U. S. Department of Energy under Contracts Nos. DOE/DE-AC02-79 ER 10364 and DOE/DE-AS02-77 ER 04215.

[1] D. J. Weber, M. A. Franey, D. Dehnhard, J. L. Artz, V. Shkolnik, and N. M. Hintz, Bull. Am. Phys. Soc. 21, 1006 (1976).
[2] C. E. Thorn, J. J. LeVine, J. J. Kolata, C. Flaum, P. D. Bond, and J. C. Sens, Phys. Rev. Lett. 38, 384 (1977).
[3] I. Y. Lee and J. X. Saladin, Phys. Rev. C 9, 2406 (1974).
[4] P. Doll, M. Bini, D. L. Hendrie, S. K. Kauffmann, J. Mahoney, A. Menchaca-Rocha, D. K. Scott, T. J. M. Symons, K. Van Bibber, M. P. Viyogi, H. Wieman, and A. J. Baltz, Phys. Lett. 76B, 566 (1978).
[5] W. G. Love, T. Terasawa, and G. R. Satchler, Phys. Rev. Lett. 39, 6 (1977); Nucl. Phys. A291, 183 (1977).
[6] A. J. Baltz, S. K. Kauffmann, N. K. Glendenning, and K. Pruess, Phys. Rev. Lett. 40, 20 (1978); Nucl. Phys. A327, 221 (1979).
[7] R. Donangelo, L. F. Canto, and M. S. Hussein, Nucl. Phys. A320, 422 (1979); Phys. Rev. C 19, 1801 (1979).
[8] P. Fröbrich, R. Lipperheide, and H. Fiedeldey, Phys. Rev. Lett. 43, 1147 (1979).
[9] P. D. Bond, M. J. LeVine, and C. E. Thorn, Phys. Lett. 68B, 327 (1977).
[10] C. R. Gruhn, T. Y. T. Kuo, C. J. Maggiore, H. McManus, F. Petrovich, and B. M. Preedom, Phys. Rev. C 6, 915 (1972).
[11] M. Buenerd, P. Martin, P. de Saintignon, and J. M. Loiseaux, Nucl. Phys. A286, 377 (1977); F. Ajzenberg-Selove, *ibid.* A248, 1 (1975).
[12] C. L. Rao, M. Reeves, and G. R. Satchler, Nucl. Phys. A207, 182 (1973); P. W. Coulter and G. R. Satchler, *ibid.* A293, 269 (1977).
[13] N. Vinh Mau and A. Bouyssy, Nucl. Phys. A257, 189 (1976).
[14] R. S. Mackintosh and A. M. Kobos, Phys. Lett. 62B, 127 (1976).
[15] P. D. Bond, C. Chasman, J. D. Garrett, C. K. Gelbke, O. Hansen, M. J. LeVine, A. Z. Schwarzschild, and C. E. Thorn, Phys. Rev. Lett. 36, 300 (1976).
[16] P. D. Kunz, computer code CHORK, modified by L. D. Rickertsen (unpublished).
[17] B.-T. Kim, Phys. Lett. 80, 353 (1979).
[18] T. Tamura, Rev. Mod. Phys. 37, 679 (1968).
[19] R. A. Eisenstein, D. W. Madsen, H. Theissen, L. S. Cardman, and C. K. Bockelman, Phys. Rev. 188, 1815 (1969).
[20] W. E. Frahn and D. H. E. Gross, Ann. Phys. (N.Y.) 101, 520 (1976).
[21] P. J. Moffa, J. P. Vary, C. B. Dover, C. W. Towsley, R. G. Hanus, and K. Nagatani, Phys. Rev. Lett. 35, 922 (1975).
[22] A. M. Lane, *Nuclear Theory* (Benjamin, New York, 1964), p. 80.
[23] M. S. Hussein, Phys. Lett. 88B, 31 (1979).